Force Generation of Curved Actin Gels Characterized by Combined AFM-Epifluorescence Measurements

Stephan Schmidt,[†‡] Emmanuèle Helfer,[§] Marie-France Carlier,[§] and Andreas Fery[†*]
[†]Physikalische Chemie II, Universität Bayreuth, Bayreuth, Germany; [‡]Interfaces Department, Max Planck Institute of Colloids and Interfaces, Potsdam-Golm, Germany; and [§]Laboratoire d'Enzymologie et Biochimie Structurales, Centre National de la Recherche Scientifque, Gif-sur-Yvette, France

ABSTRACT Polymerization of actin into branched filaments is the driving force behind active migration of eukaryotic cells and motility of intracellular organelles. The site-directed assembly of a polarized branched array forms an expanding gel that generates the force that pushes the membrane. Here, we use atomic force microscopy to understand the relation between actin polymerization and the produced force. Functionalized spherical colloidal probes of varying size and curvature are attached to the atomic force microscopy cantilever and initiate the formation of a polarized actin gel in a solution mimicking the in vivo context. The gel growth is recorded by epifluorescence microscopy both against the cantilever and in the perpendicular (lateral) nonconstrained direction. In this configuration, the gel growth stops simultaneously in both directions at the stall force, which corresponds to a pressure of 0.15 nN/μm^2. The results show that the growth of the gel is limited laterally, in the absence of external force, by internal mechanical stresses resulting from a combination of the curved geometry and the molecular mechanism of site-directed assembly of a cohesive branched filament array.

INTRODUCTION

A large number of motile processes in eukaryotic cells are mediated by site-directed assembly of actin filaments. Force is generally produced against a membrane by insertional, polarized polymerization of actin, which is initiated and controlled by a variety of protein machineries that are activated at the membrane by signaling molecules. The molecular mechanism by which these nucleation-promoting factors act plays a pivotal role in the morphology and dynamics of the force-producing actin meshworks. For instance, the processive assembly of parallel bundles of actin filaments by formins generates protrusive cellular extensions called filopodia. Flat, fan-shaped protrusions called lamellipodia, which extend in the direction of migration of crawling cells, result from the assembly of a branched filament array catalyzed by proteins of the Wiskott-Aldrich syndrome protein (WASP) family using the actin-related protein 2/3 (Arp2/3) complex. Proteins of the WASP family are also responsible for the assembly of a propulsive actin array when they act at the surface of an endocytic vesicle or an intracellular pathogen such as *Shigella* or *Listeria* (1). They are also involved in other membrane deformation processes, such as tubulation or vesicle scission linked to intracellular trafficking and organization of the Golgi. Actin assembly in dendritic branched arrays by WASP proteins produces forces that deform or propel membranes in many ways. The propulsive movement of *Shigella* and *Listeria* (2), as well as that of any solid (3–7) or soft particle (8–10) functionalized by WASP (or its neural homolog N-WASP), can be reconstituted in vitro with five pure proteins that mimic the physiological context for lamellipodium extension. The reconstituted motility assay, which is based on the concept of regulated treadmilling at the origin of motility, can be used to measure the force produced by the growth of the expanding actin gel (Fig. 1) formed by the branched filaments at the surface of the particle. In addition, analyses of mesoscopic phenomena, such as trajectories (11–13), symmetry breaking (4,14,15), and surface morphology (16–18), have provided further insights into the molecular-scale mechanisms at work in the branched actin gels. However, the relation between actin assembly and produced force is not well understood. The molecular mechanism of filament branching by surface-immobilized N-WASP-Arp2/3 machinery plays a crucial role in the motile process. In this autocatalytic filament branching reaction, N-WASP associates with the Arp2/3 complex and G-actin in a ternary complex that then interacts with one filament to nucleate a daughter filament. Each branching event thus generates two growing filaments from a single one, with the Arp2/3 complex remaining bound to the created branch junction at each cycle. A previous study (19) demonstrated that the transient links formed between particle-immobilized N-WASP and the filament meshwork determine the motile behavior. New filaments are continuously created by branching at the surface. They then detach from the surface-bound N-WASP and grow for a transient period of time until they are capped at their barbed ends by a capping protein, which disables further monomer addition. Thus, in the presence of a capping protein (gelsolin; see Materials and Methods), the actin assembly occurs exclusively at a submicrometer distance from the nucleating surface (4,7,20). Furthermore, the steady balance sustained between branching and capping maintains a constant branching density in the meshwork,

Submitted September 21, 2009, and accepted for publication January 26, 2010.

*Correspondence: andreas.fery@uni-bayreuth.de

Editor: Feng Gai.

0006-3495/10/05/2246/8 $2.00

doi: 10.1016/j.bpj.2010.01.055

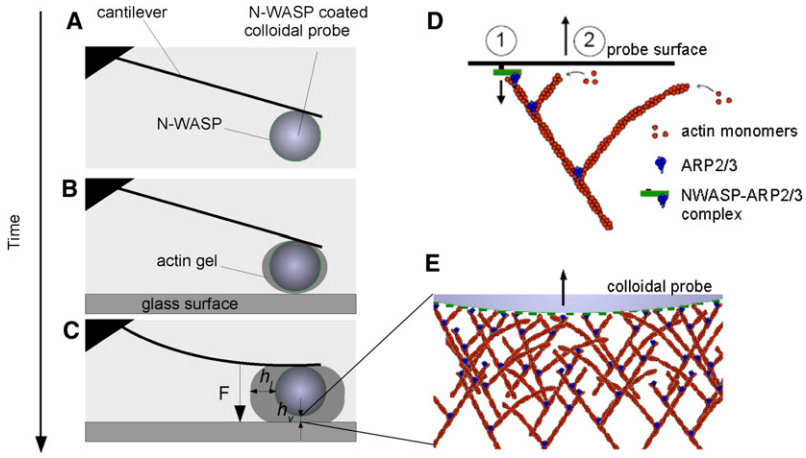

FIGURE 1 Actin gel growth from an AFM colloidal probe and force generation. (*A–C*) Schematic presentation of the measurement procedure. (*A*) An N-WASP-coated colloidal probe is glued in buffer to a tipless AFM cantilever. (*B*) After addition of the actin medium, the probe is approached to the glass slide surface, and the cantilever chip (*gray triangle*) is held in constant separation from the glass slide. (*C*) As the actin gel extends from the colloidal probe, it deflects the cantilever, which is used as a measure of force. The restoring force of the cantilever is directed against vertical growth of the actin gel. During collection of the force data, the cantilever position is kept at a constant height. The parameters h_l and h_v respectively denote the lateral and vertical gel thickness. (*D*) After activation (No. 1) by the WASP/Scar proteins, the Arp2/3 complex and actin monomers form a branched elongating actin filament that generates forces against the surface (No. 2). (*E*) A sketch of the branched actin network in the proximity of the colloidal probe (not to scale).

a stationary number of growing filament ends in the vicinity of the functionalized site, and a constant velocity of the propelled particle.

The actin meshwork is a so-called physical gel that is held together by dipolar interactions, ionic interactions, and hydrogen bonding between the filaments. Because of their dendritic assembly, the filaments entangle and form a reticulated structure that is able to generate and withstand shear stresses. Several models have been proposed to describe force generation by actin gels on different length scales. Molecular models, such as the Brownian ratchet model (21) and the filament end-tracking model (22,23), describe how directed forces emerge from elongating filaments. On the mesoscopic scale, the elastic gel model (24) provides an illustrative picture of how force can be generated against a convex-shaped object. The insertional addition of actin monomers generates consecutive actin gel layers on the object surface. As a result, the outer layer is tangentially stretched while internal layers keep building up. The tangential stress leads to a normal stress against the object surface, and has been proposed to contribute in a break in symmetry and polarized movement, or, in some cases, the arrest of gel growth. Although in vitro reconstruction of expanding actin gels was developed a decade ago, only a relatively small number of physical experimental studies on the underlying forces have been reported (6,25–27). Pioneering force-velocity measurements were performed using reconstituted motility assays under control of the viscous drag force on actin propelled colloids (6,25). Direct force measurements were conducted on an elongated *Listeria*-like comet via micropipettes (26), and an atomic force microscopy (AFM)-based technique (27) revealed a force-velocity relationship similar to that suggested by the tethered Brownian ratchet model (21). These techniques were also extended to measure the viscoelastic properties of gels (28) and friction upon gel extension (29). However, an overlooked aspect of direct actin force measurements is the effect of the gel size and morphology. Theoretical considerations, as well as experiments, suggest a dependence of generated force on gel curvature. For example, the results of bead assays indicate that motility is enhanced for smaller beads propelled by gels with larger curvatures (5). This is supported by the elastic gel model (24), which predicts that curvature-induced elastic stresses lead to larger propulsive forces. Furthermore, experiments with deformable lipid vesicles (9) and droplets (10) reveal elastic stresses in the gel due to the curved gel geometry. These elastic stresses are also responsible for the break in symmetry of spherical gel layers (14), as well as cessation of the gel expansion around spherical colloids (18). It is not known how these multiple curvature-induced effects (i.e., decelerated gel growth and elastic stresses) affect the generation of force against an external load.

In this work, we developed a method based on a combination of colloidal probe AFM and epifluorescence microscopy to directly measure the force generated by expanding actin gels of varying size and (convex) curvature. The force measurements are conducted on reconstituted actin gels in a medium consisting of purified proteins. A colloidal probe is functionalized with N-WASP, glued to the AFM cantilever tip, and placed at a given distance from the coverslip in a reconstituted motility medium containing fluorescently labeled actin, Arp2/3, and regulators of treadmilling to generate the branched array at the surface of the probe. The force measurement is combined with simultaneous analysis of the gel shape via epifluorescence imaging. This allows the gel extension against the load to be recorded simultaneously with the unconstrained extensions parallel to the load, thus enabling analysis of the elastic constants and stresses. The colloidal probe configuration in combination with in vitro reconstruction allows quantification of the biophysical boundary conditions (e.g., gel density and shape).

At small external loads, we find that the gel expansion is largely independent of the applied forces, which is consistent with results for noncurved actin gels (27). At larger loads, we observe stalling of the gel expansion. However, this growth stalling differs from that observed in noncurved gels, in that

the generation of force against the load is limited by curvature-induced mechanical stress rather than by the restoring force against the gel. The results allow estimation of the internal mechanical stress in the gel, and generally show the effect of geometric confinement on actin polymerization.

MATERIALS AND METHODS

Instrumental setup

Measurements were performed on a Nanowizard I atomic force microscope (JPK Instruments AG, Berlin, Germany) with the sample contained in a closed liquid cell (Small Cell; JPK Instruments AG). The atomic force microscope was combined with an optical microscope (Axiovert 200; Carl Zeiss AG, Göttingen, Germany) and a stage allowing for micrometer-accurate maneuvering of the cantilever during preparation. Fluorescence images were recorded using a Zeiss AxioCam HRm camera and a 20×, 0.75 NA, Zeiss Plan Aprochromat objective. The images were processed using ImageJ (30) (for processing procedures, see Fig. S1 in the Supporting Material).

Preparation of the force probe

As colloidal probes, we used either carboxylated polystyrene beads (Polysciences, Warrington, PA) with a radius of 5.5 ± 0.39 μm and 9.5 ± 0.39 μm, or larger colloidal probes (21.2 ± 0.5 μm) selected from a batch of polydisperse (30–50 μm) glass beads (Microparticles GmbH, Berlin, Germany). The colloidal probes were functionalized by physical adsorption of N-WASP to the surface. The functionalization protocol was adapted from motility assays conducted to study the movement of actin-propelled polystyrene beads (6). The probes were incubated for 1 h on ice in a functionalization solution consisting of A buffer (10 mM Hepes, pH 7.8, 0.1 M KCl, 1 mM $MgCl_2$, 1 mM ATP, 0.1 mM $CaCl_2$) supplemented with 0.5 μM N-WASP. To obtain an identical average surface density of N-WASP on beads of different diameters, the colloid suspensions were adjusted to a final total surface area of 10^9 μm^2/mL in the functionalization solution. Some variability in the N-WASP surface density could nevertheless occur from bead to bead in the same batch. After 1 h, bovine serum albumin (BSA, 10 mg/mL) was added for another 15 min to block free adsorption sites. The probes were sedimented and washed twice with A buffer and finally stored in A buffer supplemented with 1 mg/L BSA to avoid unspecific interactions and bead aggregation. The spring constants of the cantilevers (CSC 12, μMash; Estonia) with a nominal spring constant of 0.03 N/m were determined using the thermal noise method (31) or the Sader method (32). The results of both methods agreed within 10%, and values of the spring constants were in the range reported by the manufacturer. For each measurement run, a single probe was attached to an AFM cantilever using epoxy resin (UHU Schnellfest; UHU GmbH & Co. KG, Baden, Germany). Probe attachment was performed directly in the AFM liquid cell with a well-defined volume (usually 20–25 μL) of buffer A containing the probes. After curing of the epoxy resin (10 min) was completed, the force probe preparation was finished and the experiments were initiated by injecting the actin medium into the liquid cell.

Actin medium

The composition of the actin medium was identical to the optimized solution for reconstituted actin-based motility of polystyrene beads (6). The following final medium composition was obtained: 5 μM F-actin, 2.4 μM profilin, 100 nM gelsolin, 100 nM ARP2/3, and 2.2 μM ADF. The buffer system consisted of 10 mM Hepes pH 7.8, 0.1 M KCl, 4 mM $MgCl_2$, 3 mM ATP, 0.05 mM $CaCl_2$, 0.025 mM EGTA, 10 mg/mL BSA, 0.005 wt% NaN_3, 6 mM DTT, and 0.15 mM DABCO (all final concentrations).

RESULTS

For experiments, the N-WASP functionalized colloidal probe is glued to the AFM cantilever directly in the AFM liquid cell. Polymerization is started by injecting the actin medium into the liquid cell (see Materials and Methods). After the injection, actin filaments start to grow at the (g-actin|ARP2/3|N-WASP) complex bound to the surface of the colloidal probe. The resulting actin network remains attached to the probe by transient bonds between the filaments and the surface-bound N-WASP (19). After a short period of equilibration and mixing (2 min), the colloidal probe is brought into contact with the glass slide surface. The cantilever chip and glass slide are then separated for the rest of the measurement run (Fig. 1, *A–C*). In the course of the experiment, the surface bound gel grows around the colloidal probe, increasing its thickness. The part of the gel confined between the colloidal probe and the glass substrate will extend against the cantilever and deflect it (see Fig. 1 *C*). The force (F) exerted by the extending gel is derived from the actin growth-related cantilever deflection, which is measured with nanometer precision using the AFM optical lever technique. Control measurements showed that the cantilever drift was negligible as compared with the actin-based deflection of the cantilever (see Section SD in the Supporting Material). The colloidal probe configuration provides a well-controlled sphere/plate geometry. Also, the actin gel remains attached around the entire colloidal probe, adding to position stability and preventing lateral gel sliding upon increased compression forces. Moreover, the colloidal probes can be easily functionalized and selected according to their size, providing a convenient way to vary the resulting gel size and curvature. In parallel with the force measurement, the setup permits bottom-view images of the fluorescently labeled actin gel to be recorded by epifluorescence microscopy (see Fig. 2 *A*). By combining fluorescence microscopy and AFM, one can determine the lateral gel extension (h_l) and vertical gel extension (h_v), respectively.

Arrest of the lateral unconstrained gel growth correlates with arrest of the constrained growth against the cantilever

Collection of the force data is started after addition of the actin and equilibration for a short time (2 min). The probes are approached to the glass substrate until the cantilever imposes an initial force of 5 nN on the nascent gels. Once this initial force is reached, the separation between the cantilever chip and glass slide is kept fixed (constant position of the AFM z-piezo). The growing actin gel then displaces the cantilever by the deflection C. The cantilever acts like a Hookean spring, imposing a restoring force against the gel of k_cC, where k_c is the spring constant of the cantilever. Fig. 2 *B* shows a representative measurement of the cantilever deflection over time t (*black curve*), which yields $F(t)$

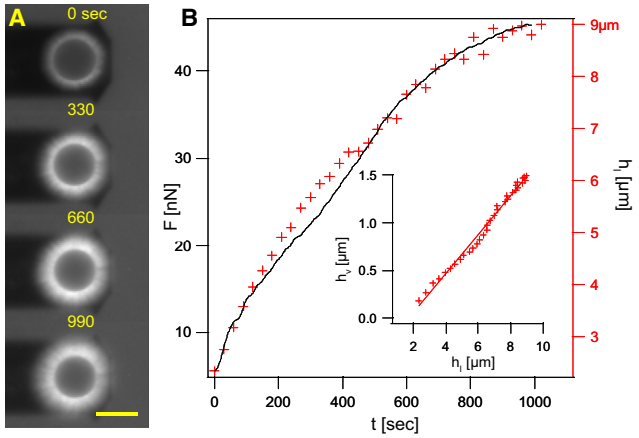

FIGURE 2 Expansion of the actin gel and generation of force. (*A*) Fluorescence microscopy images of the expanding actin gel (rhodamine-labeled). Scale bar denotes 20 μm. (*B*) The force curve $F(t) \cong h_v(t)k_c$ (*solid line*) and the lateral gel thickness h_l (+ signs) to the growing actin gel shown in *A*. The second black axis on the left side of the graph shows the cantilever deflection C, which is approximately equal to h_v. The force curve shows in a linear regime from $t = 100$ s to $t = 600$ s and a stalling regime from $t = 600$ s to $t = 1000$ s. The regimes appear simultaneously in $F(t)$ and $h_l(t)$. Inset: Plot of F versus h_l with a linear fit ($R^2 = 0.994$) indicates that the relative changes of vertical and lateral gel growth are very similar.

and, respectively, the vertical gel extension $h_v(t)$ as $C \cong h_v$ (it is not strictly equal, because a thin gel layer that is grown before the probe touches the glass slide is not considered in *C*). The recorded force curve, and in fact the whole set of measurements, show two distinct regimes. First, we observe a regime of constant force generation, i.e., a linear increase of the force. This suggests that here the gel deflects the cantilever steadily and keeps growing constantly against increasing restoring forces, at a rate of 0.16 μm/min. This growth rate is an order of magnitude smaller than the propulsion rates of beads in motility assays (typically 1–3 μm/min). In the second regime, at increased gel thickness and restoring force of the cantilever, the force levels off due to cessation of the vertical gel extension against the cantilever.

Simultaneous epifluorescence imaging of the expanding gels (Fig. 2 *A*) is used to measure the corresponding lateral gel thicknesses h_l. Because of the absence of a sharp outer gel boundary, we arbitrarily define h_l as the separation between the probe surface and the radial position where the fluorescence intensity is decreased to 25% from the maximum intensity at the probe surface (Fig. S1). The lateral gel growth as represented by h_l is shown in Fig. 2 *B* (*red markers*). We find that h_l shows the same features as h_v, i.e., a linear regime followed by leveling off. The gel extension against the cantilever h_v is smaller by a factor of six- to eightfold than the unconstrained gel extension parallel to the cantilever (h_l), but both parameters show the same relative change over time, as shown by the linear correlation between h_v and h_l (Fig. 2 *B*, *inset*).

Gel expansion and force generation are controlled by actin treadmilling

We proceed with testing the effect of different gel sizes on force generation upon gel expansion. The gel size can be easily controlled by varying the probe size. Here we measure the forces using colloidal probes of three different radii, $R_p = 5.5$, 9.7, and 21.2 μm. The results of the force and lateral thickness measurements are shown in Fig. 3 *A* and *B*, respectively (black, red, and green curves and markers correspond to measurements with $R_p = 5.5$, 9.7, and 21.2 μm, respectively). The set of force curves shows increasing maximum forces F^{max} for larger probes. Gels formed by the largest probes ($R_p = 21.2$ μm) generate the largest forces ($F^{max} = 142 \pm 14.3$ nN, averaged). However, given the large scattering of the force curves, the differences in F^{max} of the small and medium-sized probes are not obvious: 40.2 ± 8.4 nN for $R_p = 9.7$ μm, and 30.2 ± 12.4 nN ($R_p = 5.5$ μm). Taking the probes' half-sphere surface facing the substrate as the area, we obtain maximum pressures of 0.15 ± 0.045 nN/μm^2. We assume that the large scatter is due to variations in actin density, which can be observed via fluorescence even for measurement runs with the same colloidal probe type. Uneven probe surface functionalization could be the source of different actin densities. Indeed, the probes are functionalized by nonspecific adsorption of N-WASP, and it has been observed that the surface density

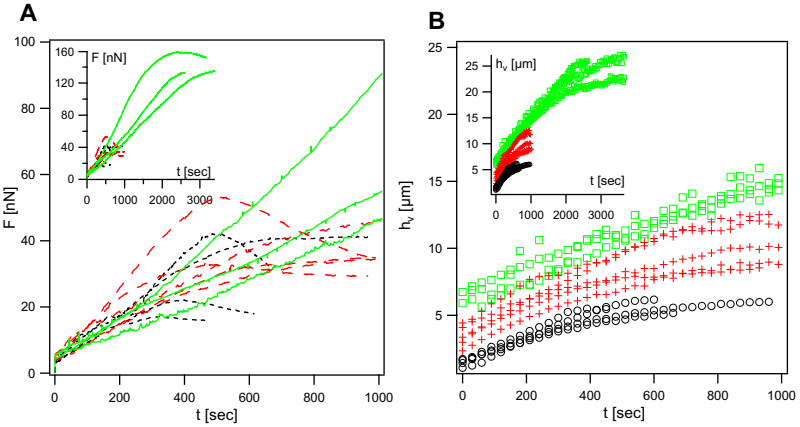

FIGURE 3 (*A*) Force versus time plot for different probe radii: 5.5 μm (*short dashed lines*), 9.5 μm (*long dashed lines*), and 21.2 μm (*solid lines*). The inset shows the complete force range for the largest probes. (*B*) Lateral actin gel thicknesses for the different probes: 5.5 μm (○), 9.5 μm (+), and 21.2 μm (□). The gel growth speed as well as the force generation rate are reduced at increased gel thicknesses and vanish at the end of every measurement.

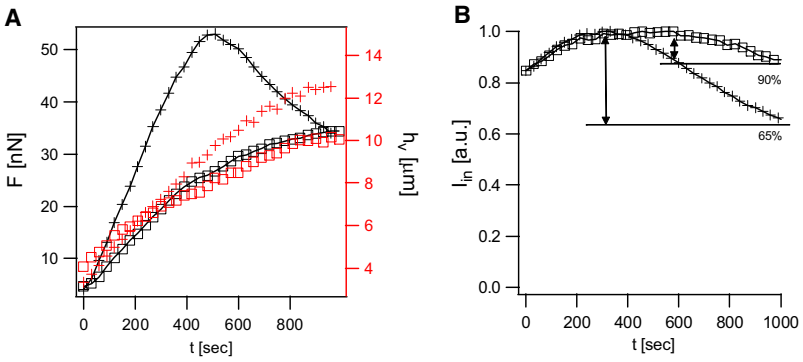

FIGURE 4 Declining forces are linked to depletion of actin between colloidal probe and the glass slide. (*A*) Comparison of a declining (+) and nondeclining (□) force curve (*lines with symbols*) with the corresponding lateral gel thicknesses h_v (symbol only). For declining forces, h_v keeps growing after F^{max} is reached, whereas for nondeclining forces, h_v follows the force curve. (*B*) The fluorescence intensity for a declining force curve (+) shows a strong decrease to 65% of the maximum intensity. The nondeclining force (□) of the intensity decreases by only 10%.

can vary from bead to bead in the same batch, as deduced from the observation of actin comets of varying densities in motility assays. Moreover, as the filaments are multiplied by autocatalytic branching at the surface, even small changes of N-WASP density on the surface can induce variations in the density of the branched actin gel and in the rate of propulsion, i.e., in the generated force. We account for these differences by normalizing for the individual gels with their fluorescence intensity I at the time when F^{max} is reached (Fig. S2). Normalizing F^{max} reduces the error by a factor of ~2 and reveals the scaling behavior with the gel size. We also find systematic differences in the actin density depending on the probe type. For example, the smallest probes always generate denser gels as compared to the medium-sized probes. To some extent, this explains the surprisingly small differences in maximum force generated by these types of probes. The set of fluorescence-normalized force curves shows a more distinct dependence on the probe size (Fig. S3). This indicates that the actin density affects the generation of force and also suggests that the large scatter in force data is caused by differences in actin gel density.

The complete set of curves shows the same qualitative behavior as the single measurement presented above. All force curves, regardless of the probe size, show a linear regime initially, followed by a regime where the force levels off. Although values for F^{max} scatter strongly, the slope for all curves in the linear regime is similar (6.9 ± 1.7 nN/min) and is clearly independent of the size of the gel. This indicates that for small loads, the vertical gel expansion (~0.15 μm/s) is not affected by the restoring force imposed by the cantilever. The expansion depends only on the gel growth kinetics, which are similar for each run.

The corresponding lateral gel thicknesses h_l for the different colloidal probes are plotted in Fig. 3 *B*. The initial gel growth rate in the lateral direction is independent of the probe size and varies between 1.0 and 1.4 μm/min, of same magnitude as the propulsion rate of beads in motility assays (6). As for $F(t)$, all $h_l(t)$ curves recorded with the same probe type level off at the same time, and leveling off occurs more rapidly for smaller probes as well. Because the growth rate is mainly independent of the gel size, the maximum gel lateral thicknesses h_l^{max} increase with the probe size. We observe no further lateral gel growth after ≈8 and ≈30 min for the smallest and largest probes, respectively. In fact, for the majority of the measurements, h_l levels off as F^{max} is reached. However, for some measurements, the force not only stops increasing, it starts to decrease. In these cases, F levels off earlier than h_l (see Fig. 4 *A*), and it seems these events are coupled to a strong decrease in the gel density. The fluorescence intensity measurement shows a decreasing density of the gel that bears the largest load, in the section between the colloidal probe and coverslip. Indeed, the decreasing force curves also show a pronounced decreased fluorescence intensity between the probe and gel as compared to the nondecreasing force curves (see Fig. 4 *B*). For nondecreasing forces, the fluorescence intensity I_{in} is almost constant; only a 90% decrease from the maximum intensity is observed. However, decreasing forces are always coupled to a much stronger decrease in the fluorescence intensity, which levels off to ~65% in the example shown in Fig. 4. The decrease of I_{in} as the force builds up indicates that the polymerization of actin is inhibited, whereas the depolymerization is not. Hence, at elevated compression forces, the gel disassembles in the section between the colloidal probe and glass. A more exhaustive discussion about the correlation between fluorescence intensity and generation of force can be found in Fig. S4.

Our interpretation (and clearly the general case) is that the vertical and lateral gel expansions stop simultaneously, which is reflected by the fact that $F(t)$ and show the same characteristics. As already observed for $F(t)$, the slope in linear regime is also similar for all $h_l(t)$ curves, meaning that here both the force and the lateral gel expansion are independent of the probe size. Further, both the F and h_l parameters level off at the same time. This strongly suggests that the gel extension against the cantilever h_v and the transduced forces are not stalled by the restoring force of the cantilever; rather, they are passively stalled due to cessation of the global gel growth. Therefore, both the initial regime, where force and growth rates are constant and thus independent of the load, and the stalling regime are controlled only by polymerization kinetics. It is important to note that the cessation of gel growth is not due to depletion of ATP or any other

essential polymerization component. Bead assays in similar actin media showed that the polymerization velocity was constant for >8 h (13).

DISCUSSION

To clarify the reason for the cessation of gel growth, we consider mechanical stresses present in the gel. As explained in the Introduction, the dendritic actin gels studied here are formed by an intricate network of branched filaments with physical cross-links. Because of this cohesive structure, actin networks generate stresses as they expand from spherical objects (e.g., colloidal beads (33)). Gel layers are formed at the nucleating probe surface and are pushed outward and stretched as new layers of actin gel are continuously formed. Stretching the cross-linked gel layers causes shear stress, which is maximal at the exterior gel layer. Continuum mechanical models predict that polymerization/depolymerization rates and consequently force generation are affected by these stresses (18). Another possible cause of growth constraints is the diffusion limitations of monomers or ARP2/3 to the probe surface. To distinguish between stress and diffusion limitation, we test whether the actin gels are under mechanical stress.

First, we perform a direct test on a gel that has generated its maximum force and is unable to displace the cantilever further. In this situation, we quickly withdraw the cantilever over a defined distance and measure the response of the gel. If the actin gel were deformed by mechanical stress, we would expect a fast response due to elastic expansion. Fig. 5 shows a force curve of a gel (probe $R_p = 5.5\ \mu m$) that has been stalled at a vertical gel thickness of 1 μm. As seen in the previous experiments, the lateral gel extension is six- to eightfold higher. If we suppose that the gel is a purely elastic body, and assume the same rates for lateral and vertical gel expansion, the gel would be strongly compressed vertically, with the strain being on the order of 85%. Clearly, this assumption is overly simplistic because the growth rate against the force is smaller than in the unconstrained lateral direction, but a part of the apparent deformation is due to elastic strain. If we now withdraw the z-piezo by 1 μm upward, the cantilever deflection decreases as expected by roughly 1 μm. This means the cantilever deflection vanishes and the compression force is reduced to almost zero. The actin gel then extends very rapidly in the vertical direction, and h_v increases almost instantaneously by 200 nm after the cantilever is withdrawn. The gel literally snaps back, which can only be explained by fast elastic gel expansion (and not by slow actin polymerization). However, the actin gel does not fully recover by fast expansion. It does not reach the maximum force again, and the lateral gel expansion is still much larger (= 4.8 μm). Also, the fast expansion is followed by slow expansion to 500 nm in h_v after the cantilever is withdrawn. This indicates that the apparent gel strain before the force reduction is not caused by elastic compression of the gel alone. It seems the growth of the compressed gel segment is inhibited. Then, since the actin medium is still around, gel growth resumes after the compression is released in conjunction with fast elastic expansion of the gel. Nevertheless, the fast gel expansion indicates that the gel is in a state of elastic stress. A similar experiment by Parekh et al. (27) on actin gels grown from a planar geometry showed enhanced polymerization velocity as the cantilever was retracted. However, they did not report a quasi-instantaneous response for the curved actin gels, as observed here.

Another indication of mechanical stresses can be found by using elasticity theory, i.e., by analyzing the scaling of maximum lateral gel thickness h_l^{max} with probe radius R_p. In the case of elastic limitation, more strongly curved gels (smaller probes) generate smaller gel thicknesses and vice versa. Noireaux et al. (18) showed that h_l^{max} scales linearly with R_p as $h_l^{max} \cong B^{1/2} R_p$, where B is a factor that balances the chemical driving force with the mechanical stress storage in the gel. On the other hand, if the gel growth were diffusion-limited, h_l^{max} would be insensitive to changes in R_p. The gel thickness h_l^{max} is linearly dependent on R_p (Fig. 6), suggesting that the gel growth is limited by mechanical stresses rather than by diffusion. Such a linear behavior is consistent with previous studies on actin gel symmetry breakage and comet formation under similar conditions (5,14). For the ratio of the lateral gel expansion to the bead size, h_l^{max}/R_p, we obtained 1.2, which is much larger than that reported previous work. For example, van der Gucht et al. (14) obtained 0.2, whereas using ActA-coated beads Noireaux et al. (18) obtained 0.075 as the bead/gel thickness ratio. Besides differences in the medium composition, the unusually large gel thickness found here could be the result

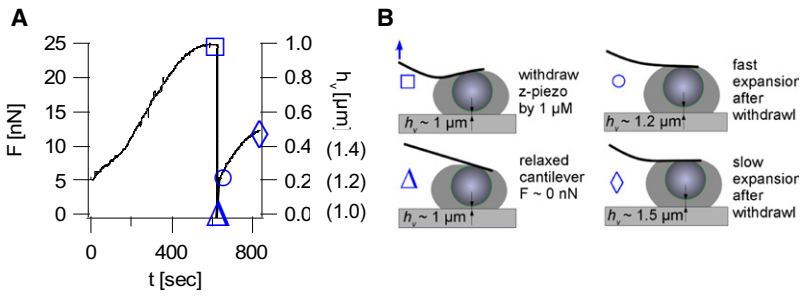

FIGURE 5 Actin gels are governed by internal elastic stresses. (*A*) The force curve levels off due to cessation of the vertical growth. The gel shows fast vertical expansion after withdrawal of the cantilever, due to release of mechanical tension. The gel pushes the cantilever by 200 nm instantaneously after withdrawal. The final vertical gel extension h_v^{max} is 1.5 μm, from $h_v = 1\ \mu m$ before cantilever withdrawal plus $\Delta h_v = 0.5\ \mu m$ after withdrawal. (*B*) Illustration of the experiment.

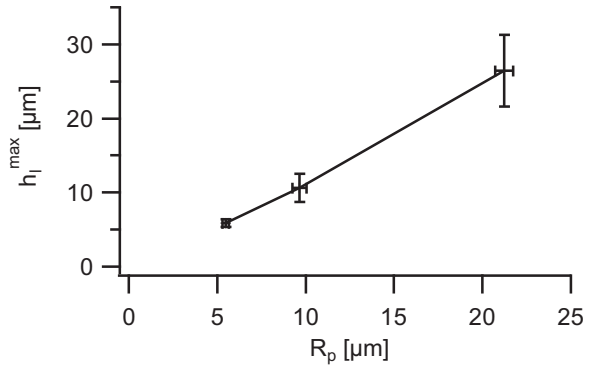

FIGURE 6 The maximum gel thickness in the lateral direction h_l^{max} at which the actin gel ceases to expand and to generate force as a function of the probe radius. The linear behavior shows that h_l^{max} is limited by elastic stresses, but not by diffusion or depletion of ATP.

of a preexisting symmetry break, i.e., from the contact of the probes with the cantilevers.

An analysis of elastic stress buildup in actin gels grown on spherical colloids (18) shows that the tangential stress, or shear stress, $\sigma_{\perp\perp}$ due to stretching of the previously grown gel layer is maximal at the gel exterior and zero at the probe surface (Fig. 7). The radial stress σ_{rr} is maximal at the probe surface and, in the absence of external forces, vanishes at the gel exterior. Here, the restoring force of the cantilever gives rise to the radial stress of the gel compartment in between the colloidal probe and the glass slide. Thus, the AFM force measurements can be used to estimate the radial stress contribution σ_{est} of the gel layer in contact with the glass slide surface. We use the ratio of maximum force F^{max} and the contact area A^{max} (using the limiting gel thickness) to determine σ_{est}. The choice of the contact area A^{max} is a bit arbitrary due to the diffuse gel boundary. We define the gel boundary of the stationary gel at the position where the fluorescence intensity is decreased to 25% (see Fig. S1) Nevertheless, we find increasing σ_{est} as the probe size is decreased: 94 Pa (R_p = 5.5 μm); 39 Pa (R_p = 9.5 μm); and 25 Pa (R_p = 21.2 μm) (standard deviations are on the order of 20%). The measured

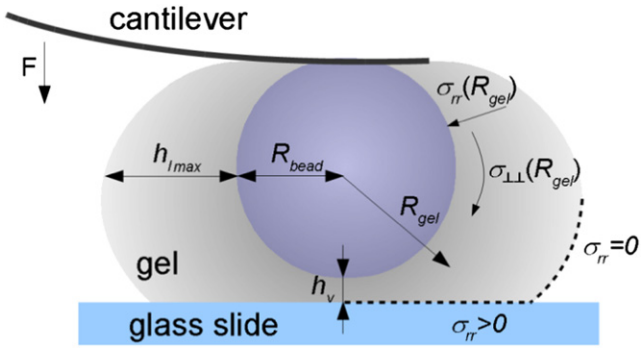

FIGURE 7 Sketch of the mechanical stresses $\sigma_{\perp\perp}$ and σ_{rr}, and other parameters used in the text to describe the state of an actin gel growing against a cantilever.

stresses σ_{est} are due to the radial stress contribution and can be projected to the bead surface facing the substrate, thus generating a force against the AFM cantilever. The larger radial stresses for smaller gel curvatures are reminiscent of the enhanced propulsive force of smaller actin-propelled colloids as compared to larger ones (5).

In conclusion, using colloidal probe AFM measurements, we studied the force generation and expansion of spherical actin gels confined against a load. At the same time, we measured the gel extension in the uncompressed direction parallel to the load, and investigated the effect of gel size and curvature. Remarkably, the resulting stalling forces and the corresponding pressures (0.15 $\pm$ 0.045 nN/μm^2) were an order of magnitude smaller than measurements obtained on noncurved, stress-free actin gels (26,27). We suggest that for spherical gels, as studied here, the gel extension and force generation are counteracted by the internal gel stress, whereas the gel extension in a nonspherical configuration is stalled by the external force. The scaling behavior of the maximum gel expansion with the colloidal probe size provides evidence that the gel is indeed in a state of elastic stress. In the range of convex curvatures tested here, all gels showed a cessation of force generation due to internal mechanical stress rather than external force. There are also indications that the generation of force is hindered by decreasing filament density in the region of large stress. The AFM-probe geometry and the expanding gels can be adapted to mimic other biological counterparts, such as the concave-shaped lamellipodium of crawling cells. Furthermore, with this technique, one can obtain force measurements while varying the gel composition. The results should provide further insight into the role of mediating proteins, such as the capping protein or ARP2/3, during actin-based generation of force. Due to the lack of internal stresses, nonreticulated actin networks generated by formins should show no self-arresting gel expansion. Investigators could use approaches similar to the one presented here to elucidate the roles played by various actin-binding proteins in the mechanics of such gels, e.g., by studying formin-coated probes and controlled integration of actin filament cross-linkers.

SUPPORTING MATERIAL

Five figures are available at http://www.biophysj.org/biophysj/supplemental/S0006-3495(10)00220-1.

The authors thank Georg Freund and Walter Zimmermann for discussions, and Dominique Didry and Diep Le (members of M.-F.C.'s group) for providing the purified proteins. E.H. and M.-F.C. belong to the CNRS Consortium CellTiss.

This study was supported by grants from the Deutsche Forschungsgemeinschaft Forschergruppe 608, European Community STREP Active Biomics, l'Agence Nationale de la Recherche Physique et Chimie du Vivant (to M.-F.C.), l'Agence Nationale de la Recherche (09-JCJC-0040, to E.H.), and Ligue Nationale Contre le Cancer (Équipe Labellisée).

REFERENCES

1. Pollard, T. D., and G. G. Borisy. 2003. Cellular motility driven by assembly and disassembly of actin filaments. *Cell*. 112:453–465.
2. Loisel, T. P., R. Boujemaa, …, M. F. Carlier. 1999. Reconstitution of actin-based motility of *Listeria* and *Shigella* using pure proteins. *Nature*. 401:613–616.
3. Cameron, L. A., M. J. Footer, …, J. A. Theriot. 1999. Motility of ActA protein-coated microspheres driven by actin polymerization. *Proc. Natl. Acad. Sci. USA*. 96:4908–4913.
4. Delatour, V., S. Shekhar, …, M. F. Carlier. 2008. Actin-based propulsion of functionalized hard versus fluid spherical objects. *N. J. Phys.* 10:025001.
5. Bernheim-Groswasser, A., S. Wiesner, …, C. Sykes. 2002. The dynamics of actin-based motility depend on surface parameters. *Nature*. 417:308–311.
6. Wiesner, S., E. Helfer, …, D. Pantaloni. 2003. A biomimetic motility assay provides insight into the mechanism of actin-based motility. *J. Cell Biol*. 160:387–398.
7. Akin, O., and R. D. Mullins. 2008. Capping protein increases the rate of actin-based motility by promoting filament nucleation by the Arp2/3 complex. *Cell*. 133:841–851.
8. Boukellal, H., O. Campas, …, C. Sykes. 2004. Soft *Listeria*: Actin-based propulsion of liquid drops. *Phys. Rev. E Stat. Nonlin. Soft Matter Phys.* 69:061906/1–061906/4.
9. Upadhyaya, A., J. R. Chabot, …, A. van Oudenaarden. 2003. Probing polymerization forces by using actin-propelled lipid vesicles. *Proc. Natl. Acad. Sci. USA*. 100:4521–4526.
10. Giardini, P. A., D. A. Fletcher, and J. A. Theriot. 2003. Compression forces generated by actin comet tails on lipid vesicles. *Proc. Natl. Acad. Sci. USA*. 100:6493–6498.
11. Shaevitz, J. W., and D. A. Fletcher. 2007. Load fluctuations drive actin network growth. *Proc. Natl. Acad. Sci. USA*. 104:15688–15692.
12. Cameron, L. A., J. R. Robbins, …, J. A. Theriot. 2004. Biophysical parameters influence actin-based movement, trajectory, and initiation in a cell-free system. *Mol. Biol. Cell*. 15:2312–2323.
13. Schmidt, S., J. van der Gucht, …, A. Fery. 2008. Non-Gaussian curvature distribution of actin-propelled biomimetic colloid trajectories. *Eur. Biophys. J*. 37:1361–1366.
14. van der Gucht, J., E. Paluch, …, C. Sykes. 2005. Stress release drives symmetry breaking for actin-based movement. *Proc. Natl. Acad. Sci. USA*. 102:7847–7852.
15. Dayel, M. J., O. Akin, …, R. D. Mullins. 2009. In silico reconstitution of actin-based symmetry breaking and motility. *PLoS Biol*. 7:e1000201.
16. Schwartz, I. M., M. Ehrenberg, …, J. L. McGrath. 2004. The role of substrate curvature in actin-based pushing forces. *Curr. Biol.* 14:1094–1098.
17. Bernheim-Groswasser, A., J. Prost, and C. Sykes. 2005. Mechanism of actin-based motility: a dynamic state diagram. *Biophys. J*. 89:1411–1419.
18. Noireaux, V., R. M. Golsteyn, …, C. Sykes. 2000. Growing an actin gel on spherical surfaces. *Biophys. J*. 78:1643–1654.
19. Delatour, V., E. Helfer, …, G. Romet-Lemonne. 2008. Arp2/3 controls the motile behavior of N-WASP-functionalized GUVs and modulates N-WASP surface distribution by mediating transient links with actin filaments. *Biophys. J*. 94:4890–4905.
20. Paluch, E., J. van der Gucht, …, C. Sykes. 2006. Deformations in actin comets from rocketing beads. *Biophys. J*. 91:3113–3122.
21. Mogilner, A., and G. Oster. 2003. Force generation by actin polymerization II: the elastic ratchet and tethered filaments. *Biophys. J*. 84:1591–1605.
22. Dickinson, R. B. 2009. Models for actin polymerization motors. *Proc. Int. Conf. Indust. Appl. Math., Zurich. 81–103*.
23. Dickinson, R. B. 2009. Diffusion-limited speed of an actin-propelled particle near a surface. *Cell. Mol. Bioeng*. 2:200–206.
24. Gerbal, F., P. Chaikin, …, J. Prost. 2000. An elastic analysis of *Listeria* monocytogenes propulsion. *Biophys. J*. 79:2259–2275.
25. McGrath, J. L., N. J. Eungdamrong, …, S. C. Kuo. 2003. The force-velocity relationship for the actin-based motility of *Listeria* monocytogenes. *Curr. Biol*. 13:329–332.
26. Marcy, Y., J. Prost, …, C. Sykes. 2004. Forces generated during actin-based propulsion: a direct measurement by micromanipulation. *Proc. Natl. Acad. Sci. USA*. 101:5992–5997.
27. Parekh, S. H., O. Chaudhuri, …, D. A. Fletcher. 2005. Loading history determines the velocity of actin-network growth. *Nat. Cell Biol.* 7:1219–1223.
28. Chaudhuri, O., S. H. Parekh, and D. A. Fletcher. 2007. Reversible stress softening of actin networks. *Nature*. 445:295–298.
29. Marcy, Y., J. F. Joanny, …, C. Sykes. 2007. Probing friction in actin-based motility. *N. J. Phys*. 9:7.
30. Rasband, W. S. 1997–2009. ImageJ. http://rsb.info.nih.gov/ij/. U.S. National Institutes of Health, Bethesda, MD.
31. Hutter, J. L., and J. Bechhoefer. 1993. Calibration of atomic-force microscope tips. *Rev. Sci. Instrum*. 64:1868–1873.
32. Sader, J. E. 1998. Frequency response of cantilever beams immersed in viscous fluids with applications to the atomic force microscope. *J. Appl. Phys*. 84:64–76.
33. Julicher, F., K. Kruse, …, J. F. Joanny. 2007. Active behavior of the cytoskeleton. *Phys. Rep*. 449:3–28.